Nanostructure Changes in Lung Surfactant Monolayers Induced by Interactions between Palmitoyloleoylphosphatidylglycerol and Surfactant Protein B†

Junqi Ding,‡ Ivo Doudevski, Heidi E. Warriner, Timothy Alig, and Joseph A. Zasadzinski*

Department of Chemical Engineering, University of California, Santa Barbara, California 93106-5080

Alan J. Waring

Department of Medicine, UCLA, Los Angeles, California 90095, and Department of Pediatrics Harbor-UCLA, Torrance, California 90502

Mark A. Sherman

Division of Biology, Beckman Research Institute, City of Hope Medical Center, Duarte, California 91010

Received July 1, 2002. In Final Form: October 4, 2002

Developing synthetic lung surfactants to replace animal extracts requires a fundamental understanding of the roles of the various lipids and proteins in native lung surfactant. We used Brewster angle microscopy (BAM), atomic force microscopy (AFM), and Langmuir isotherms to study the influence of palmitoyloleoylphosphatidylglycerol (POPG) in monolayers of dipalmitoylphosphatidylcholine and palmitic acid mixtures with or without dSP-$B_{1-25,}$ a peptide dimer based on the first 25 amino acids of surfactant protein B (SP-B). At surface pressures between 30 and 40 mN/m, only monolayers containing POPG and dSP-B_{1-25} showed plateaus in the isotherm similar to those in Survanta, a bovine extract replacement lung surfactant that contains native SP-B and SP-C proteins. BAM images show distinct morphological changes in the fluid phase during these plateaus, while AFM images of deposited monolayers show that multilayer structures, which we named "nanosilos", form in the fluid phase at the plateau. These nanosilos are from 50 to 300 nm in diameter and from 5 to 8 nm in height and are similar to those observed in deposited Survanta monolayers. We propose that POPG and SP-B interact to stabilize the monolayer composition by trapping POPG in three-dimensional surface-associated aggregates at high surface pressures, preventing the irreversible loss of POPG and SP-B to the subphase.

Introduction

Proper lung function requires a low surface tension to minimize the work of breathing and ensure uniform lung inflation.[1−6] The low tensions are provided by molecular films of lung surfactant, a complex mixture of lipids and specific proteins that lines the liquid−air interface in the lung alveoli. Lung surfactants include saturated and unsaturated phosphatidylcholines (PC) and phosphatidylglycerols (PG), with smaller amounts of phosphatidylethanolamines (PE), phosphatidylserines (PS), and cholesterol.[7,8] In addition, four surfactant proteins known as SP-A, SP-B, SP-C, and SP-D make up about 10 wt % of native surfactant;[8] of the four, SP-B and SP-C are known to be surface active. A lack of functional lung surfactant in premature infants can lead to respiratory distress syndrome (RDS), a potentially fatal condition. Replacement lung surfactants derived from natural and synthetic sources have significantly reduced neonatal mortality caused by RDS.[9] In the United States, one of the most commonly used clinical replacement surfactants is Survanta, a bovine lung surfactant extract supplemented with palmitic acid, triglycerides, and dipalmitoylphosphatidylcholine (DPPC) that contains the amphipathic surfactant proteins SP-B and SP-C.[7] Hence, the properties of Survanta are appropriate benchmarks against which to judge the phase behavior and morphology of new synthetic replacement surfactants and protein mimetic peptides.

Of the four known surfactant specific proteins, SP-B is the only one that is absolutely required for postnatal lung

* To whom correspondence should be addressed. Phone: 805-893-4769. Fax: 805-893-4731. E-mail: gorilla@engineering.ucsb.edu.

† Part of the *Langmuir* special issue entitled The Biomolecular Interface.

‡ Current address: Unilever Research US, 45 River Road, Edgewater, NJ 07020. E-mail: junqi.ding@unilever.com.

(1) Notter, R. H. *Lung surfactants*: *Basic science and clinical applications*; Marcel Dekker: New York, 2000; Vol. 149.
(2) Body, D. R. *Lipids* **1971**, *6*, 625−629.
(3) Rooney, S. A.; Canavan, P. M.; Motoyama, E. K. *Biochim. Biophys. Acta* **1974**, *360*, 56−67.
(4) Shelley, S. A.; Balis, J. U.; Paciga, J. E.; Espinoza, C. G.; Richman, A. V. *Lung* **1982**, *160*, 195−206.
(5) Shelley, S. A.; Paciga, J. E.; Balis, J. U. *Lipids* **1984**, *19*, 857−862.
(6) Yu, S.; Harding, P. G. R.; Smith, N.; Possmayer, F. *Lipids* **1983**, *18*, 522−529.
(7) Bernhard, W.; Mottaghian, J.; Gebert, A.; Rau, G. A.; von der Hardt, H.; Poets, C. F. *Am. J. Crit. Care Med.* **2000**, *162*, 1524−1533.
(8) Goerke, J. *Biochim. Biophys. Acta-Molecular Basis of Disease* **1998**, *1408*, 79−89.
(9) Robertson, B.; Halliday, H. L. *Biochim. Biophys. Acta* **1998**, *1408*, 346−361.

10.1021/la0261794 CCC: $25.00
Published on Web 11/12/2002

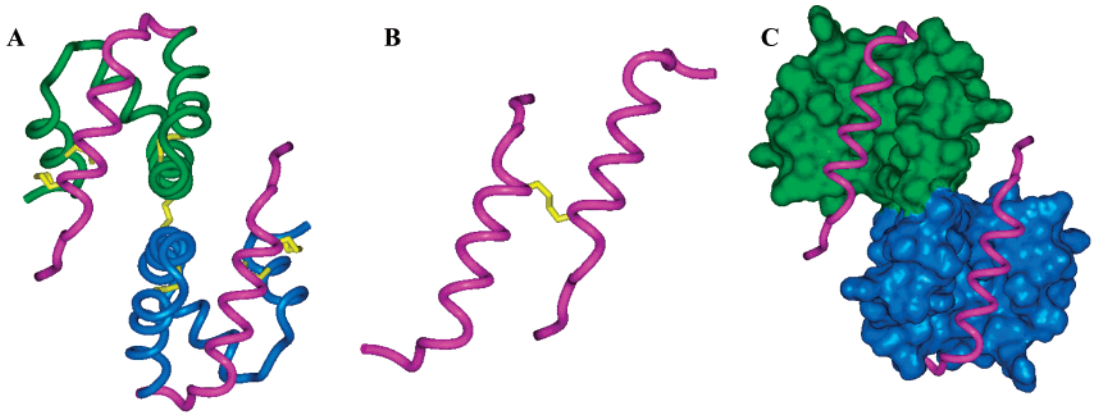

Figure 1. (A) The hypothetical structure of the native SP-B homodimer based on the model of Zaltash et al. (ref 44). The 25-residue N-terminal insertion domain is shown in red tubes with the remaining mid- and C-terminal sequences in blue and green and the disulfide connectivity in yellow. (B) The corresponding dSP-B_{1-25} mimetic peptide is shown in red with the disulfide linkage in yellow. (C) Connolly molecular surface representation (ref 62) in green and blue of the native SP-B homodimer molecular model with the 25-residue N-terminal insertion domain in red tubular format.

function and survival.[1,10,11] Complete deficiency of SP-B in mice and humans results in lethal, neonatal RDS.[1,12,13] SP-B is a 78-residue, lipid-associating protein found in mammalian lung surfactant at concentrations of about 2 wt % and is considered to be a member of the saposins, a family of proteins that associate with lipids, have a highly α-helical secondary structure, and share common disulfide connectivities.[14−16] Each SP-B monomer has disulfide links at the midsequence, N-terminal, and C-terminal sections, suggesting the main chain may assume a hairpinlike format. The native SP-B protein has a net positive charge of 8 (10 cationic and 2 anionic residues), a large fraction of strongly hydrophobic residues, and four amphipathic helical segments with the helical axes oriented parallel to the interface. The optimal in vitro and in vivo activity of SP-B in lung surfactant lipid dispersions has been associated with the homodimeric form of the protein.[17] A molecular model of the native full length SP-B homodimer is shown in Figure 1.

The orientation of the N-terminal amphipathic helix on the surface of the SP-B protein suggests that this helix may be important to the interaction of the dimeric form of the protein with surfactant lipids in monolayers and lipid dispersions.[11,18] To test this hypothesis, we synthesized a homodimeric peptide of the N-terminal domain (Figure 1) consisting of the insertion sequence (residues 1−7) and the amphipathic helix (residues 8−25) as a mimic to the native SP-B. The dimer, which we call dSP-B_{1-25}, emulates many features of the full length SP-B homodimer in vitro.[19,20] Here we show that dSP-B_{1-25} interacts specifically with fluid-phase palmitoyloleoylphosphatidylglycerol (POPG) in mixed monolayers, similar to the native SP-B,[21] and leads to morphologies similar to those seen in Survanta monolayers that contain the native SP-B.

Although the concentration and sequence of the lung surfactant proteins is highly conserved between animal species, the lipid composition of native surfactant is quite variable.[7] Moreover, the composition variations between different clinically used replacement surfactants are amplified by the nature of extraction from the animal sources and the choice of "additives".[7] Even so, a limited number of lipid components are generally agreed to be essential to surfactant performance in vivo and simplify the choices for model systems.[8,9] The lipids common to all lung surfactants are saturated DPPC and unsaturated phosphatidylcholines and phosphatidylglycerols.[22] Palmitic acid, while found at low concentrations in native surfactants,[22] is a common additive to replacement surfactants such as Survanta.[7]

The most abundant lipid in all native and replacement surfactants, DPPC, forms a semicrystalline monolayer capable of surface tensions near zero when fully compressed at physiological temperature. However, used alone, it fails as a lung surfactant[9,23] as it is slow to adsorb from aqueous suspension and respreads slowly when compression is relieved. It is likely that the unsaturated phospholipids and hydrophobic proteins in native surfactant are present to address these limitations of DPPC monolayers.[22,24,25]

The anionic phosphatidylglycerols in lung surfactant have attracted special attention because this class of phospholipids is not common in mammalian cells and is more typical of bacterial membranes. In vivo[26] studies point to a central role for PG in surfactant function. Replacement surfactant without PG does not seem to stabilize the alveoli of the newborn as well as does surfactant with PG.[1] Moreover, human studies have shown

(10) Weaver, T. E.; Conkright, J. J. *Annu. Rev. Physiol.* **2001**, *63*, 555−578.
(11) Walther, F. J.; Gordon, L. M.; Zasadzinski, J. A.; Sherman, M. A.; Waring, A. J. *Mol. Genet. Metab.* **2000**, *71*, 342−351.
(12) Weaver, T. E.; Beck, D. C. *Biol. Neonate* **1999**, *76*, 15−18.
(13) Akinbi, H. T.; Breslin, J. S.; Ikegami, M.; Iwamoto, H. S.; Clark, J. C.; Whitsett, J. A.; Jobe, A. H.; Weaver, T. E. *J. Biol. Chem.* **1997**, *272*, 9640−9647.
(14) Munford, R. S.; Sheppard, P. O.; Ohara, P. J. *J. Lipid Res.* **1995**, *36*, 1653−1663.
(15) Liepinsh, E.; Andersson, M.; Ruysschaert, J. M.; Otting, G. *Nat. Struct. Biol.* **1997**, *4*, 793−795.
(16) Andersson, M.; Curstedt, T.; Jornvall, H.; Johansson, J. *FEBS Lett.* **1995**, *362*, 328−332.
(17) Beck, D. C.; Ikegami, M.; Na, C.-L.; Zaltash, S.; Johansson, J.; Whitsett, J. A.; Weaver, T. E. *J. Biol. Chem.* **2000**, *275*, 3365−3370.
(18) Walther, F. J.; Hernandez-Juviel, J.; Bruni, R.; Waring, A. J. *Am. J. Respir. Crit. Care Med.* **1997**, *156*, 855−861.
(19) Bringezu, F.; Ding, J.; Brezesinski, G.; Waring, A.; Zasadzinski, J. A. *Langmuir* **2002**, *18*, 2319−2325.
(20) Veldhuizen, E. J.; Waring, A. J.; Walther, F. J.; Batenburg, J. J.; van Golde, L. M.; Haagsman, H. P. *Biophys. J.* **2000**, *79*, 377−384.
(21) Ding, J. Q.; Takamoto, D. Y.; von Nahmen, A.; Lipp, M. M.; Lee, K. Y. C.; Waring, A. J.; Zasadzinski, J. A. *Biophys. J.* **2001**, *80*, 2262−2272.
(22) Veldhuizen, R.; Nag, K.; Orgeig, S.; Possmayer, F. *Biochim. Biophys. Acta* **1998**, *1408*, 90−108.
(23) Poulain, F. R.; Clements, J. A. *West. J. Med.* **1995**, *162*, 43−50.
(24) Hawgood, S.; Derrick, M.; Poulain, F. *Biochim. Biophys. Acta* **1998**, *1408*, 150−160.
(25) Johansson, J. *Biochim. Biophys. Acta* **1998**, *1408*, 161−172.
(26) Hallman, M.; Feldman, B. H.; Kirkpatrick, E.; Gluck, L. *Pediatr. Res.* **1977**, *11*, 714−720.

that PG was absent from lung effluent in infants with respiratory distress syndrome of the newborn, whereas effluent from healthy control subjects of similar gestational age contained this phospholipid. Indeed, PG has proved to be a very useful biochemical marker for the maturity of the surfactant system in the developing fetus in a number of species.[1,27]

Studies using fluorescence anisotropy indicate that SP-B interacts selectively with the anionic PG in DPPC−dipalmitoylphospatidylglycerol (DPPG) mixed monolayers.[28] This is not surprising as SP-B has a +8 net positive charge and DPPG is negatively charged at physiological conditions. In addition to segregating on the basis of charge, SP-B is found at much higher concentrations in the fluid rather than in the condensed phases of DPPG/POPG monolayers.[29−31] Many proteins are expelled from the ordered condensed phase in monolayers in favor of the less ordered fluid phase due to packing considerations. However, recent grazing incidence X-ray diffraction showed that SP-B also affects the molecular packing in the condensed phase.[19] SP-B is believed to eliminate the selective removal or "squeeze-out" of POPG from mixed DPPG/POPG monolayers by inducing a two- to three-dimensional transformation of the fluid-phase fraction of the monolayer.[21,31,32] SP-B induces a reversible folding transition at monolayer collapse, allowing all components of surfactant to remain at the interface during respreading. The folds remain attached to the monolayer and are identical in composition and morphology to the unfolded monolayer, and a significant fraction are reincorporated into the monolayer upon expansion.[21,32] These findings were confirmed by Krol et al.[33] who showed that in mixed monolayers of DPPC and DPPG, filamentous domain boundaries occur at intermediate surface pressure (15−30 mN/m), while disklike protrusions prevail at elevated pressure (50−54 mN/m). Mixtures of SP-B and SP-C have also been shown to induce the fusion of PG vesicles.[34]

Palmitic acid (PA), while found at low concentrations in native surfactants,[22] is added to clinical replacement surfactants such as Survanta[7,35,36] to enhance performance. PA increases the order of the DPPC-rich solid domains in monolayers, leading to higher solid-phase fractions and higher transition temperatures.[37] Adding PA to DPPC/POPG mixtures dramatically increases monolayer viscosity at low surface tension[38,39] and can modify SP-C function.[21]

In this study, Langmuir isotherms, Brewster angle microscopy (BAM), and atomic force microscopy (AFM) were used to try to re-create at least some aspects of the morphology and phase behavior of Survanta with a simplified model surfactant containing a synthetic dimeric peptide, dSP-B_{1-25}, based on the SP-B protein (Figure 1). Developing a purely synthetic clinical replacement surfactant including synthetic proteins or peptides may help reduce costs, standardize formulations, improve surfactant supply, and eliminate the possibility of animal−human transmission of disease. Langmuir monolayers at the air−water interface are convenient and appropriate model systems for studies of lung surfactants and other amphiphilic molecules. Care is necessary to extrapolate Langmuir monolayer behavior to lung surfactant behavior in vivo, but general correlations between in vitro and in vivo behavior are starting to emerge.[8,21,40−43] The combination of these methods gives a better picture of the relationship of composition, organization, and structure to the essential functions of lung surfactant such as low minimum surface tension and rapid respreading.

Adding dSP-B_{1-25} to DPPC/POPG/PA monolayers induces a plateau in the isotherm similar to that in isotherms of Survanta monolayers at similar surface pressure. By varying the concentration of POPG in mixtures of DPPC/POPG/PA, we found a strong correlation between the amount of POPG and the extent of the plateaus. These plateaus in Survanta have been hypothesized to result from the selective squeeze-out or removal of the unsaturated, fluid lipids from the monolayer. BAM and AFM images show that a structure we call "nanosilos" was formed during the plateaus for the systems with dSP-B_{1-25}. The nanosilos are lipid−protein structures from 50 to 300 nm in diameter and from 5 to 8 nm in height. These nanosilos depend on the presence of both SP-B and POPG in the model lung surfactant monolayers. Similar features also are observed in Survanta monolayers that contain the native SP-B protein. We propose that interactions between SP-B and POPG stabilize monolayer composition by trapping POPG in these surface-associated three-dimensional nanosilo aggregates at higher surface pressures, preventing POPG loss from high-pressure squeeze-out even before monolayer collapse. The close similarity between the morphologies formed in the bovine extract surfactant Survanta that contains the native protein SP-B and our model lung surfactant mixtures containing dSP-B_{1-25} and POPG strongly suggests that the model surfactant mixture and synthetic peptide capture these aspects of surfactant function.

Experimental Section

Materials. 1,2-Dipalmitoyl-*sn*-glycero-3-phosphatidylcholine (DPPC) and 1-palmitoyl-2-oleyl-*sn*-glycero-3-phosphatidylglycerol (POPG) were purchased from Avanti Polar Lipids (Alabaster, AL; purity > 99%). Palmitic acid (purity > 99%) was obtained from Sigma Chemical Co. (St. Louis, MO). All samples were used without further purification. Water was prepared using a Millipore Milli-Q system and had a resistivity of >18 MΩ cm^{-1}.

Survanta was purchased from Ross Laboratories (Columbus, OH). Survanta is a natural bovine lung extract containing phospholipids, neutral lipids, fatty acids, and the surfactant-associated proteins SP-B and SP-C. To this are added DPPC, PA, and tripalmitin to standardize the Survanta composition. The approximate concentration is 25 mg/mL phospholipid (of

(27) Hallman, M.; Kulovich, M.; Kirkpatrick, E.; Sugarman, R. G.; Gluck, L. *Am. J. Obstet. Gynecol.* **1976**, *125*, 613−617.
(28) Baatz, J. E.; Elledge, B.; Whitsett, J. A. *Biochemistry* **1990**, *29*, 6714−6720.
(29) Lee, K. Y. C.; Lipp, M. M.; Zasadzinski, J. A.; Waring, A. J. *Proc. SPIE-Int. Soc. Opt. Eng.* **1998**, *3273*, 115−133.
(30) Lipp, M. M.; Lee, K. Y. C.; Zasadzinski, J. A.; Waring, A. J. *Science* (*Washington, D.C.*) **1996**, *273*, 1196−1199.
(31) Takamoto, D. Y.; Lipp, M. M.; von Nahmen, A.; Lee, K. Y. C.; Waring, A. J.; Zasadzinski, J. A. *Biophys. J.* **2001**, *81*, 153−169.
(32) Lipp, M. M.; Lee, K. Y. C.; Takamoto, D. Y.; Zasadzinski, J. A.; Waring, A. J. *Phys. Rev. Lett.* **1998**, *81*, 1650−1653.
(33) Krol, S.; Ross, M.; Sieber, M.; Kunneke, S.; Galla, H.-J.; Janshoff, A. *Biophys. J.* **2000**, *79*, 904−918.
(34) Shiffer, K.; Hawgood, S.; Duzgunes, N.; Goerke, J. *Biochemistry* **1988**, *27*, 2689−2695.
(35) Tanaka, Y.; Takei, T.; Kanazawa, Y. *Chem. Pharm. Bull.* **1983**, *31*, 4100−4109.
(36) Tanaka, Y.; Takei, T.; Aiba, T.; Masuda, K.; Kiuchi, A.; Fujiwara, T. *J. Lipid Res.* **1986**, *27*, 475−485.
(37) Bringezu, F.; Ding, J.; Brezesinski, G.; Zasadzinski, J. A. *Langmuir* **2001**, *17*, 4641−4648.
(38) Ding, J.; Warriner, H. E.; Zasadzinski, J. A. *Langmuir* **2002**, *18*, 2800−2806.
(39) Ding, J.; Warriner, H. E.; Zasadzinski, J. A. *Phys. Rev. Lett.* **2002**, *88*, 168201−168204.
(40) Johansson, J.; Curstedt, T. *Eur. J. Biochem.* **1997**, *244*, 675−689.
(41) Schürch, S.; Green, F. H. Y.; Bachofen, H. *Biochim. Biophys. Acta* **1998**, *1408*, 180−202.
(42) Zasadzinski, J. A.; Ding, J.; Warriner, H.; Bringezu, F. *Curr. Opin. Colloid Interface Sci.* **2001**, *6*, 506−513.
(43) Warriner, H. E.; Ding, J.; Waring, A.; Zasadzinski, J. A. *Biophys. J.* **2002**, *82*, 835−842.

which 60−75 wt % is DPPC), 0.5−1.75 mg/mL triglycerides, and 1.5−3.5 mg/mL free fatty acids. Survanta contains lower concentrations of SP-B and SP-C than native surfactant due to losses during the extraction process.[7]

The N-terminal dimeric precursor peptide (Figure 1) was synthesized on a 0.25 mmol scale with an ABI 431A peptide synthesizer using Fmoc chemistry as described previously.[20] The amino acid sequence is reported elsewhere.[21] Solvents and ion pairing agents were removed from the peptide fractions followed by lyophilization from acetonitrile/10 mM HCl (1/1 v/v). Dimeric SP-B_{1-25} (dSP-B_{1-25}) was prepared from the monomeric precursor using trifluoroethanol/10 mM phosphate buffer, pH 7.5 (1/1 v/v).[20] The expected molecular mass was confirmed by fast atom bombardment mass spectrometry, electrospray and MALDI mass spectrometry (UCLA Center for Molecular and Medical Mass Spectrometry, Los Angeles, CA). The full length native human SP-B homodimer and dSP-B_{1-25} peptide were modeled using Insight/Discover 98.0 software (Molecular Simulations, San Diego, CA) on a Silicon Graphics Indigo-2R10000 High Impact workstation (Beckman Research Institute, City of Hope Core Facility). A hypothetical model for the full length SP-B homodimer was constructed by templating the SP-B amino acid sequence on the known 2-D NMR structure of a closely related saposin protein, NK-lysin (PDB: 1NKL), similar to that described by Zaltash et al.[44] and Walther et al.[11] The dSP-B_{1-25} homodimer was constructed using two SP-B_{1-25} monomers from the coordinates for the peptide in the Protein Data Bank (PDB: 1DFW).[45] Cys-11 was mutated to alanine and the Cys-8 of one monomer was covalently linked to the Cys-8 of a second monomer to form a disulfide linkage as described by Bringezu et al.[19]

Methods. The pressure−area isotherms were collected using a custom-built Langmuir trough equipped with a Wilhelmy type pressure-measuring device and a computer-controlled barrier.[46] Survanta was diluted in 0.9% sodium chloride solution at a total concentration of about 2 mg/mL. The Survanta suspension was spread at the interface by depositing small drops of the aqueous suspension onto the subphase surface. Monolayer spreading solutions (∼0.5 mg/mL) of the synthetic model surfactant were prepared by mixing the desired amount of individual stock solutions of DPPC, POPG, and PA in chloroform/methanol (4/1 v/v). This solution was then spread dropwise onto a pure water subphase to form monolayers; the initial compressions were begun after about 10 min to allow for complete evaporation of the solvent. Two mixtures were used: one without dSP-B_{1-25} (**MA**) and one with dSP-B_{1-25} (**MB**). The following are the relative weight ratios for each sample: **MA1**, DPPC/POPG/PA = 45/45/8; **MA2**, DPPC/POPG/PA = 50/40/8; **MA3**, DPPC/POPG/PA = 55/35/8; **MA4**, DPPC/POPG/PA = 60/30/8; **MA5**, DPPC/POPG/PA = 65/25/8; **MA6**, DPPC/POPG/PA = 70/20/8; **MA7**, DPPC/POPG/PA = 75/15/8; **MA8**, DPPC/POPG/PA = 80/10/8; **MB1**, DPPC/POPG/PA/dSP-B_{1-25} = 45/45/8/10; **MB2**, DPPC/POPG/PA/dSP-B_{1-25} = 50/40/8/10; **MB3**, DPPC/POPG/PA/dSP-B_{1-25} = 55/35/8/10; **MB4**, DPPC/POPG/PA/dSP-B_{1-25} = 60/30/8/10; **MB5**, DPPC/POPG/PA/dSP-B_{1-25} = 65/25/8/10; **MB6**, DPPC/POPG/PA/dSP-B_{1-25} = 70/20/8/10; **MB7**, DPPC/POPG/PA/dSP-B_{1-25} = 75/15/8/10; **MB8**, DPPC/POPG/PA/dSP-B_{1-25} = 80/10/8/10.

Brewster Angle Microscopy. An argon ion laser (Coherent) was used as the light source. An adjustable mirror and a Glen-Thompson polarizer (Melles-Griot, Sunnyvale, CA) placed between laser and trough provided p-polarized light at the Brewster angle (53.1° from vertical for a pure water surface).[46−48] A simple biconvex lens (Melles-Griot) was used to collect the reflected light. An additional polarizer was used as an analyzer in order to improve contrast and determine changes in molecular tilt angle in the monolayer. Images were collected using a Sony CCD camera (model XC-75), recorded using a JVC super VHS VCR (Elmwood Park, NJ), and processed using a custom computerized data acquisition system.

Atomic Force Microscopy. Silicon wafers and freshly cleaved mica were used as substrates for deposition. The silicon wafers were cleaned in a hot "piranha" solution (H_2O_2/H_2SO_4, 3:7 v/v) to remove organic contaminants while leaving the native oxide intact and then stored in clean water until used. Mica substrates were cleaved with ordinary adhesive tape immediately before use. No differences in transfer or monolayer morphology were observed between the two substrates.

To deposit monolayers, we modified the inverted Langmuir−Schaefer transfer technique,[49] which allows for the continuous fluorescence imaging of the monolayer during transfer from the air−subphase interface to the substrate. The advantages of this deposition technique are that it is simple and inexpensive and can be implemented in almost all Langmuir troughs; moreover, any artifacts associated with nonideal transfer can readily be identified. However, in the original process, the substrate is attached to a magnetic stainless steel disk. The disk is held by a magnet at the center of a stainless steel base fitted with a sharp-edged stainless steel ferrule. The magnetic steel disk is glued to the substrate, which may cause contamination when the epoxy contacts the subphase. In addition, the commercial stainless steel ferrule is too large for the deposition; the monolayer contained inside the ferrule is deformed during the deposition. In our new design, instead of using a magnet to fix the substrate, four small posts keep the substrate from moving. Figure 2 shows the schematic and a photo of the deposition device. A 15° knife edge was machined to cut the monolayer at a prescribed area per molecule when the subphase level was lowered. The distance from the knife edge to the substrate top surface is kept small to prevent the monolayer from deforming during deposition.

A modified Nanoscope III AFM (Digital Instruments, Santa Barbara, CA) was used for imaging in ambient conditions. The samples were glued or taped to magnetic stainless steel disks, which were then attached to the piezoelectric tube scanner via an internal magnet on the scanner. AFM imaging was done with a 150 μm × 150 μm (J) scanner in contact mode. Silicon nitride tips with a spring constant of 0.12 N/m were used. Exerting large forces on the sample was a concern during imaging, so samples were checked often for deformation. This was done by imaging for a few minutes on a smaller region (∼20 μm) and then zooming out to check whether damage had been done to the scanned region.

Results

The starting point of the study is the morphology and phase behavior of Survanta monolayers. Isotherms of Survanta have been published earlier[21] and show a plateau at a surface pressure from about 40−50 mN/m at 37 °C. At 25 °C, the plateau occurs at a lower surface pressure around 40 mN/m as shown in Figure 3A. This plateau has generally been ascribed to the squeeze-out or selective removal of unsaturated, fluid-phase lipids from the monolayer[1] or to the formation of SP-C-induced multilayers.[21] Figure 3B,D shows AFM images of Survanta monolayers transferred at a surface pressures below the plateau pressure onto mica substrates; the samples shown in Figure 3C,E were transferred above the plateau pressure. Below the plateau, the images consist of distinct domains of different heights, corresponding to the coexistence of condensed and fluid-phase monolayers. The continuous fluid phase (dark gray) is about 1 nm lower than the condensed-phase islands (lighter gray). Islands of condensed phase (10−100 nm scale) are distributed at a low density in the fluid phase as can be seen in the higher magnification view in Figure 3D. Other than these features, both phases in the monolayer are quite flat over micrometers in extent. Above the plateau pressure, Figure 3C shows that the fluid-phase regions are compressed in size and the condensed-phase islands are surrounded by small protrusions, 50−300 nm diameter and 5−8 nm

(44) Zaltash, S.; Palmblad, M.; Curstedt, T.; Johansson, J.; Persson, B. *Biochim. Biophys. Acta-Biomembranes* **2000**, *1466*, 179−186.
(45) Gordon, L. M.; Lee, K. Y.; Lipp, M. M.; Zasadzinski, J. A.; Walther, F. J.; Sherman, M. A.; Waring, A. J. *J. Pept. Res.* **2000**, *55*, 330−347.
(46) Lipp, M. M.; Lee, K. Y. C.; Waring, A.; Zasadzinski, J. A. *Biophys. J.* **1997**, *72*, 2783−2804.
(47) Henon, S.; Meunier, J. *Rev. Sci. Instrum.* **1991**, *62*, 936−939.
(48) Honig, D.; Mobius, D. *Thin Solid Films* **1992**, *210/211*, 64−68.
(49) Lee, K. Y. C.; Lipp, M. M.; Takamoto, D. Y.; Ter-Ovanesyan, E.; Zasadzinski, J. A. *Langmuir* **1998**, *14*, 2567−2572.

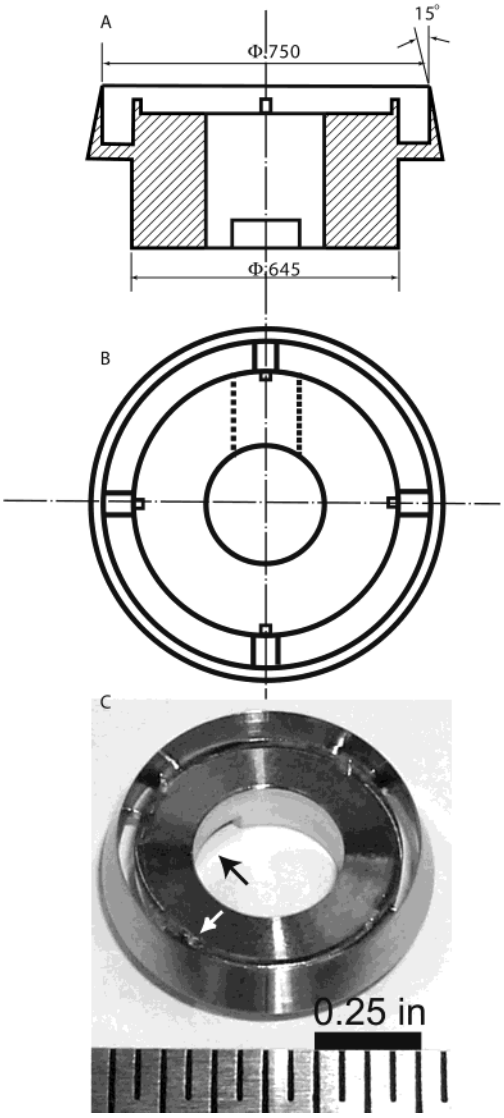

Figure 2. (A) Top and (B) side schematic diagrams and (C) a photo of the deposition stage. The stage is constructed of stainless steel. Four small prongs hold and center the substrate (1 cm diameter mica or silicon wafer circles, white arrow in the photo). Holes in the bottom and sides of the stage allow the subphase to slowly drain away as the subphase level is lowered in the trough, thereby depositing the monolayer onto the substrate (black arrow in the photo). A rim with a 15° knife edge cuts and holds the monolayer at a constant area/molecule, and hence surface pressure, when the subphase level is lowered. The rule is in inches.

higher than the surrounding monolayer. The white patches are located primarily in the remaining fluid phase, which is now the same height as the condensed-phase domains. Figure 3E shows more clearly the extent and size of the patches and their location between the condensed-phase islands. We had earlier attributed these patches to excess Survanta in the subphase trapped during the transfer to the mica substrate.[21] However, as the formation of the patches, which we call "nanosilos," is correlated with the plateau in the isotherms, it is clear that the nanosilos are an intrinsic feature of the Survanta monolayer. These nanosilos may be a mechanism of stabilizing the unsaturated lipids and SP-B protein in the vicinity of the monolayer for subsequent reincorporation as the monolayer is expanded. SP-C does not appear to be required for either the plateau in the isotherm or the formation of nanosilos in the model surfactant. Similar plateaus in the isotherms and nanosilos are common only to monolayers

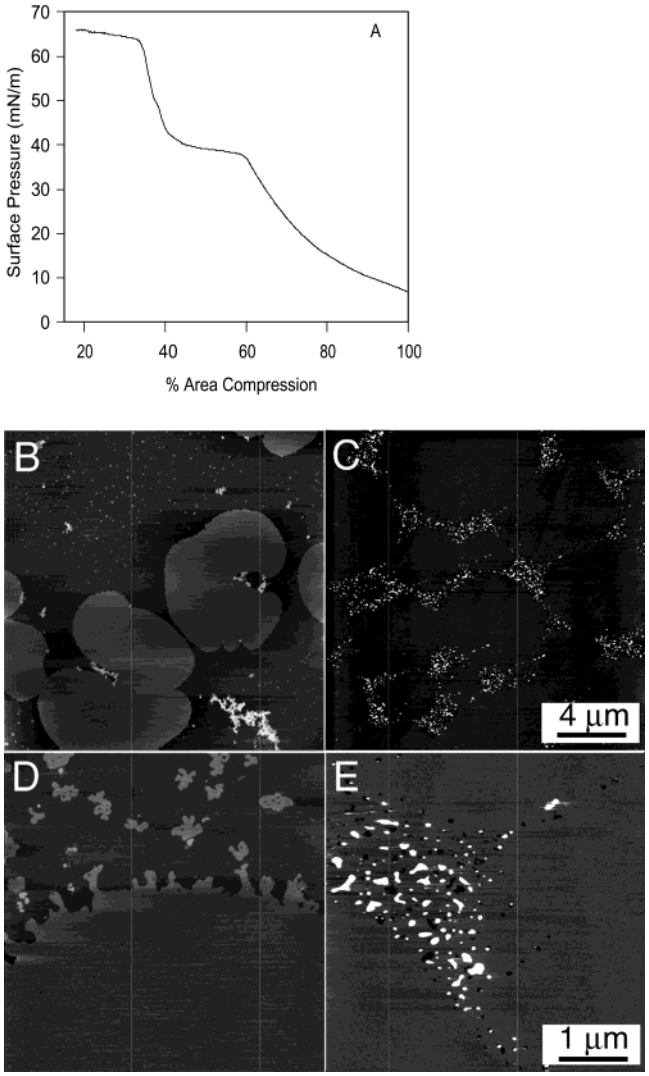

Figure 3. (A) Isotherm of a Survanta monolayer at 25 °C on a pure water subphase. The isotherm exhibits a distinct horizontal plateau at about 35−40 mN/m, followed by collapse at 66 ± 2 mN/m. The plateau occurs at about 50 mN/m at 37 °C (ref 21). (B,D) AFM images of a Survanta monolayer transferred at a surface pressure of 30 mN/m and 25.0 °C onto mica from a water subphase. This is below the plateau pressure in the isotherm in (A). The condensed-phase islands (light gray) are about 1 nm higher than the continuous fluid phase (dark gray). The fluid phase has a low density of small condensed-phase domains that are more easily resolved in the higher magnification image, (D). (C,E) AFM images of a Survanta monolayer transferred at a surface pressure of 45 mN/m and 25.0 °C onto mica from a water subphase. The low-magnification image shows that the condensed-phase islands are more closely packed and are separated by an apparently higher continuous phase. The higher magnification image (E) shows that the continuous phase is actually characterized by small, white (5−8 nm higher than background) patches scattered over the fluid phase. The fluid phase is the same height as the condensed phase. These same structures were observed in Survanta films transferred at 37 °C above the plateau pressure (ref 21). Compare these structures to the nanosilos observed in monolayers of model lung surfactants containing dSP-B_{1-25} and POPG (Figures 8−11).

containing POPG and the peptide mimic dSP-B_{1-25}, suggesting that these structures in Survanta are also due to SP-B and the unsaturated PG in native surfactant.

Pressure−Area Isotherms. Figure 4A shows the surface pressure−area isotherms of the lipid mixtures (**MA**) on a pure water subphase at 25.0 °C. Figure 4B shows pressure−area isotherms of the mixtures with dSP-

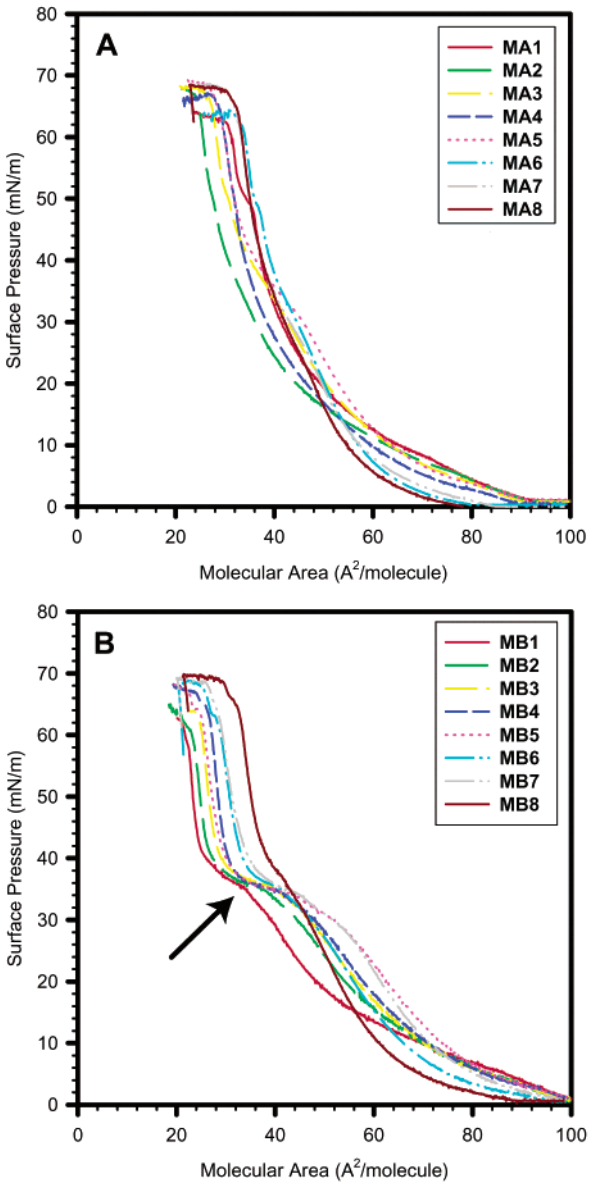

Figure 4. (A) Isotherms of lipid mixtures of DPPC/POPG/PA in different ratios at 25.0 °C on a subphase of pure water. Without dSP-B_{1-25}, the isotherms are rather similar and featureless at all POPG concentrations, except **MA1**, which has the highest POPG concentration and shows a small kink at about 50 mN/m. This kink is likely evidence of squeeze-out of some POPG, which has a collapse pressure of 48 mN/m. (B) Isotherms of lipid mixtures of DPPC/POPG/PA with dSP-B_{1-25} in different ratios at 25.0 °C on a subphase of pure water. With the peptide, plateaus between 30 and 40 mN/m can be observed for every mixture (arrow). This plateau is at a surface pressure similar to the one in Survanta monolayers (Figure 3A) and is well below the collapse pressure of POPG. The length of the plateau depends on the content of POPG in the mixtures.

B_{1-25} (**MB**) under the same conditions. Molecular areas are calculated based on the average molecular weight of all lipids in all the isotherms to highlight the differences caused by the dSP-B_{1-25}. For the lipid mixtures, lower fractions of POPG (**MA5**, **MA6**, **MA7**, **MA8**) gave a higher collapse pressure (minimum surface tension) of about 68 mN/m; at the highest POPG fractions, the collapse pressure was reduced to about 62 mN/m (**MA1**, **MA2**). There is a small kink in the isotherm around 50 mN/m for **MA1**, which contained the highest fraction of POPG. This kink likely corresponds to a partial removal or squeeze-out of the POPG, as it occurs near the 48 mN/m collapse pressure of pure POPG.[31] Other than this, there appears to be little effect on the isotherms over the rather broad range of DPPC/POPG ratios.

dSP-B_{1-25} induces an obvious change in the isotherms manifested by the distinct "plateau" between 30 and 40 mN/m in all the samples (arrow). For **MB8**, with the lowest fraction of POPG, the plateau was the smallest. For **MB5**, which contains more POPG, the plateau lengthened, although higher fractions of POPG did not increase the plateau length further. The plateau occurs at a similar surface pressure to that observed in Survanta monolayers (Figure 3A) and is well below the 48 mN/m collapse pressure of POPG.

Brewster Angle Micrographs. Figures 5 and 6 show BAM images of the lipid mixtures (**MA**) and the lipid mixtures with dSP-B_{1-25} (**MB**) on a subphase of pure water at 25.0 °C. BAM is particularly useful to follow morphology changes in the absence of any fluorescent dye. The contrast in BAM images is due to local differences in the monolayer refractive index caused by differences in local molecular density or packing.[47] Mixtures without dSP-B_{1-25} show a homogeneous, featureless field at a surface pressure of 0 mN/m, except for **MA8**, which shows isolated condensed-phase domains (brighter gray regions) even at 0 mN/m (Figure 5). For samples **MA3**−**MA7**, condensed domains appear (bright regions) at a surface pressure around 5 mN/m. For the highest fractions of POPG, **MA1** and **MA2**, condensed phase regions to do not appear until >10 mN/m. When the analyzer is rotated, the brightness of the condensed domains changes, indicating the anisotropy of the condensed phases, which is consistent with a nonzero molecular tilt angle at these PA/DPPC ratios.[37,50] The appearance of the fluid regions is unchanged as there is no long-range order or orientation to induce molecular anisotropy. The condensed-phase domains remain brighter than the fluid-phase domains at all surface pressures.

The size of the individual condensed-phase domains generally decreases as the POPG fraction increases. This is consistent with the fluidizing effect of POPG. The critical point (at which condensed phases do not occur at any surface pressure) for POPG on water is about 20 °C.[31] Below this temperature, POPG monolayers undergo a high-pressure liquid expanded (LE)/liquid condensed (LC) phase transition. For physiologically relevant conditions (above 20 °C), POPG monolayers only exhibit the LE phase, with the fluid phase existing up to collapse of the monolayer at a surface pressure of approximately 48 mN/m.[31]

The mixtures with dSP-B_{1-25} (**MB**) (Figure 6) show the same features as the mixtures without dSP-B_{1-25} at lower surface pressure, but the sizes of condensed domains are smaller. This is consistent with earlier observations that SP-B and its peptides are usually concentrated in the fluid phases.[21,31] As in the samples without dSP-B_{1-25}, the condensed domains change from dark gray to bright gray on rotating the analyzer, indicating tilted condensed-phase domains. However, the difference in contrast disappears at 35−40 mN/m, that is, for surface pressures exceeding the plateaus in the pressure−area isotherms shown in Figure 4B. X-ray diffraction of similar systems containing a monomer peptide version of SP-B also showed a decrease in tilt at higher surface pressures, leading to the decreased anisotropy in the condensed phases.[19] Surprisingly, the continuous phase (fluid phase) changed contrast on rotating the analyzer at surface pressures above the

(50) Lee, K. Y. C.; Gopal, A.; von Nahmen, A.; Zasadzinski, J. A.; Majewski, J.; Smith, S.; Howes, P. B.; Kjaer, K. *J. Chem. Phys.* **2002**, *116*, 774−783.

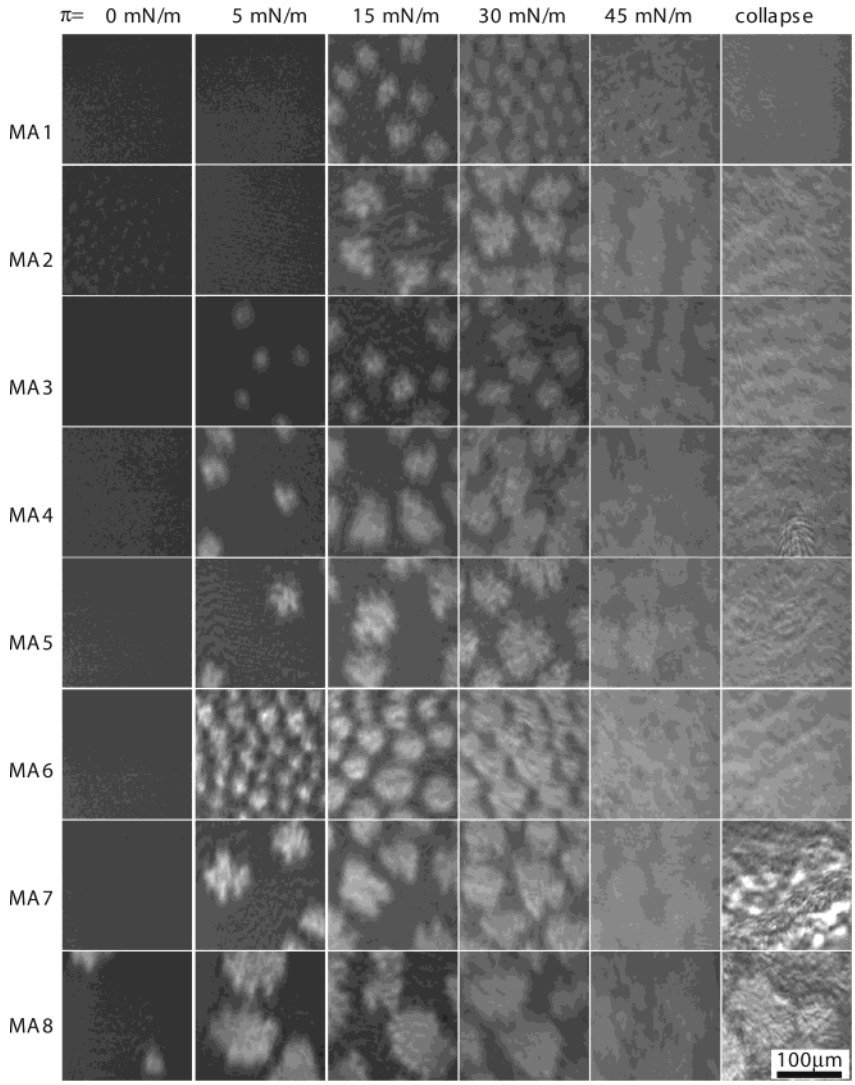

Figure 5. Brewster angle micrographs of lipid mixtures on pure water at 25.0 °C. From top to bottom, each row corresponds to single mixture; the columns give the surface pressure at which the micrographs were recorded. Contrast in the micrographs arises from coexistence of fluid (dark areas) to condensed domains (bright areas) that have different refractive indices and hence reflect more or less light at the Brewster angle. By rotation of the analyzer in the BAM, the bright, condensed-phase domains change contrast, which indicates that the molecules in the condensed phase are tilted from the vertical (ref 47). As the DPPC content is increased at a given surface pressure (e.g., 5 mN/m), the fraction of monolayer that is condensed also increased. At a certain surface pressure, contrast was lost regardless of analyzer orientation, which shows that the molecules are untilted. Similarly, as the surface pressure imposed on a given surfactant mixture is increased, the fraction of the monolayer surface occupied by condensed domains increases.

plateau, suggesting that the fluid phase was no longer isotropic but had acquired some local order. This is best seen as a reversal in contrast as the surface pressure is increased from 30 to 45 mN/m and is especially apparent in samples **MB5**−**MB8**; the condensed-phase domains switch from bright on a dark background to dark on a bright background. This change in the contrast between the fluid and condensed phases is likely due to the changes in the monolayer due to the presence of the dSP-B_{1-25}, which are more easily seen in AFM images of transferred monolayers.

Atomic Force Microscopy. Monolayers deposited at 30 mN/m and 25 °C from a pure water subphase were not significantly affected by dSP-B_{1-25} (Figure 7A,C). However, as observed in the optical micrographs, condensed domains are larger for mixtures without dSP-B_{1-25} (**MA**); domains averaged about 15 μm in diameter as opposed to about 10 μm for mixtures with dSP-B_{1-25} (**MB**). All the mixtures consistently showed isolated condensed-phase domains in a continuous fluid matrix. The condensed-phase domains were typically about 0.5−1 nm taller than the fluid phases; the domains were typically very uniform in height across the domains. The difference in height is likely a combination of the true height difference between the phases and the difference in compressibility of the two phases.[21] The shapes and distribution of the condensed phase domains were identical to those in the BAM images (Figures 5 and 6). In the continuous fluid phase, smaller domains with the same height as the larger condensed domains were distributed uniformly, suggesting that small condensed-phase domains are distributed throughout the fluid phase. Analysis of higher magnification images (data not shown) shows that these smaller domains do not depend on POPG concentration. Monolayers with dSP-B_{1-25} show similar but smaller domains distributed throughout the fluid phase (Figure 7C). As these nanometer scale condensed-phase domains are below the resolution of optical microscopy, we cannot definitely say if they are not artifacts of the transfer process, or true features of the monolayers at the air−water interface.

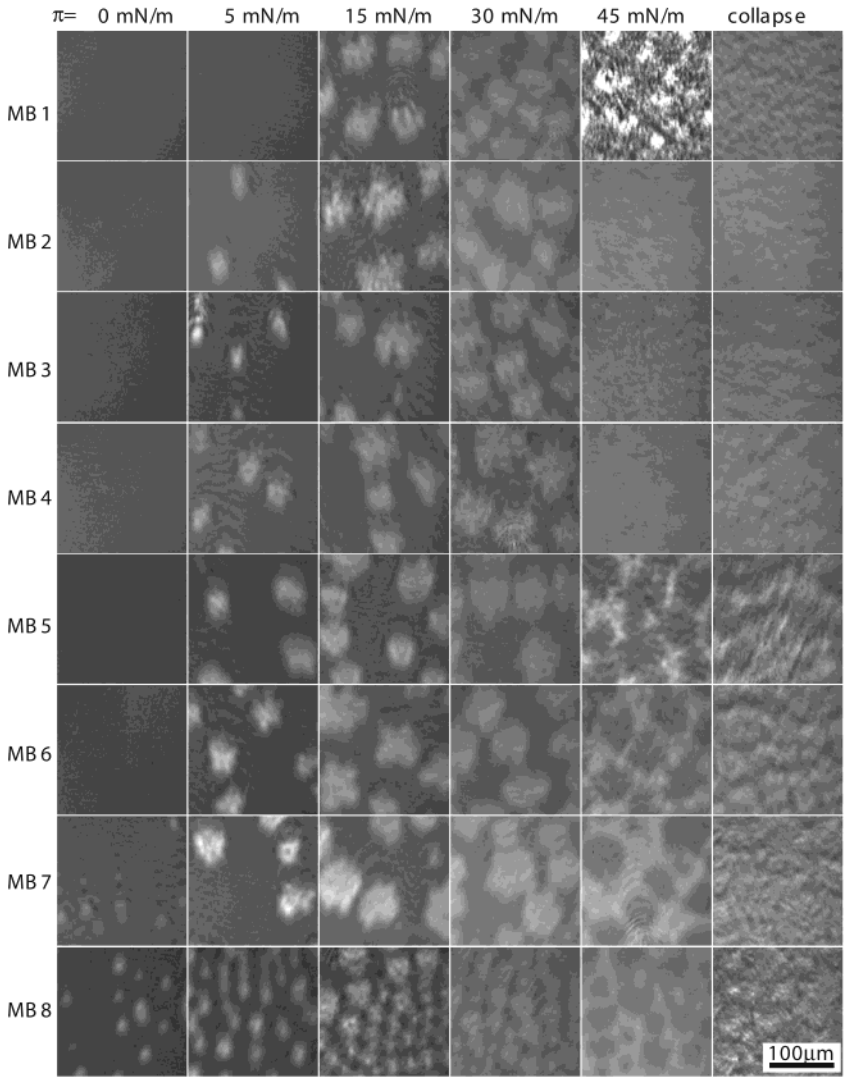

Figure 6. BAM images of lipid/dSP-B_{1-25} mixtures on pure water at 25.0 °C. As in Figure 5, from top to bottom, each row corresponds to single mixture; the columns give the surface pressure at which the micrograph was recorded. Contrast in the micrographs arises from coexistence of fluid (continuous, dark areas) to condensed domains (bright areas). By rotation of the analyzer in the Brewster angle microscope, the bright domains can change to dark domains, indicating that molecules in the solid phase are tilted with respect to the surface normal. As the content of DPPC is increased at a given surface pressure (e.g., 5 mN/m), the fraction of monolayer that is condensed also increased. At a certain surface pressure corresponding to the plateau in the $\pi-A$ isotherms in Figure 4B, the contrast was lost regardless of analyzer orientation, indicating that the molecules are untilted. At the pressure above the plateau, the dark areas and bright areas switch contrast as shown in the difference between images taken at 30 and 45 mN/m (the more DPPC, the more obvious the effect). When the analyzer is rotated, the continuous phase changes from dark to bright while the condensed domains remain dark. This suggests that the continuous phase at high pressures develops a degree of molecular anisotropy, which may be caused by the nanosilos seen in Figures 8 and 9.

At 40 mN/m, mixtures without dSP-B_{1-25} still maintain a continuous fluid phase surrounding the condensed domains (Figure 7B). The appearance of the condensed domains is very similar to that observed at a deposition pressure of 30 mN/m. However, the area fraction of the fluid phase is reduced, and the small condensed-phase structures previously observed in the fluid phase now form a more distinct and apparently connected network.

Figure 8 shows AFM images of deposited monolayers of mixtures with dSP-B_{1-25} at 40 mN/m (**MB**), just above the plateau pressure (Figure 4B). These images are strikingly different from those obtained for monolayers without dSP-B_{1-25} (Figure 7A,C) and for the same monolayers at a surface pressure below that of the plateau (Figure 7B). The condensed domains, which are still identifiable by their distinctive flower shape, now appear darker than the surrounding phase. The surrounding phase, which may or may not be a true fluid phase at this pressure, consists of randomly distributed white (higher) patches on a uniformly dark background. Those dots, which we call nanosilos, are common to all monolayers with dSP-B_{1-25} deposited at 40 mN/m (Figure 8). Expanding the monolayers to surface pressures below the plateau causes these nanosilos to disappear. Hence, formation of nanosilos appears to be a reversible process that explains the plateaus in the isotherms of the films containing dSP-B_{1-25}. Higher magnification images (the bottom row in Figure 8) show that the lateral dimensions of the nanosilos range from 50 to 300 nm and height traces show that the tops of the silos are from 5 to 8 nm above the background phase. Above the plateau pressure, the height difference between the fluid and solid phases is reduced to zero.

To clarify the effect of individual lipid components on the formation of nanosilos, monolayers with one or more of the lipids removed were imaged after deposition from 25 °C and 40 mN/m (Figure 9). Figure 9A shows an AFM image of a DPPC/PA/dSP-B_{1-25} (75/8/10) mixture. The proportion of fluid phase is greatly reduced as expected

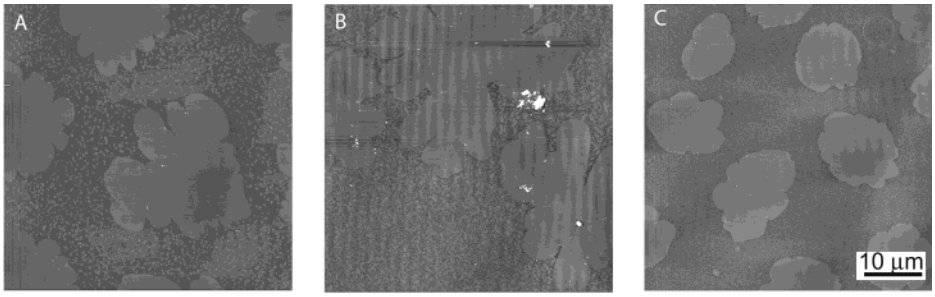

Figure 7. Atomic force micrographs of deposited monolayers on mica surfaces. (A) Image of monolayer **MA2** (DPPC/POPG/PA = 50/40/8) deposited at 30 mN/m at 25.0 °C. The continuous phase (fluid phase in the monolayer) is lower than the domains (solid phase) by about 1 nm. This image is recovered after expansion and recompression of the films. (B) The monolayer **MA2** (DPPC/POPG/PA = 50/40/8) deposited at 40 mN/m at 25.0 °C still has the lower continuous phase and higher domains. (C) The monolayer **MB2** (DPPC/POPG/PA/dSP-B_{1-25} = 50/40/8/10) deposited at 30 mN/m (below the plateau in the isotherm) at 25.0 °C also has the lower continuous phase and higher solid domains. Below the plateau, there are virtually no morphological changes induced by dSP-B_{1-25}.

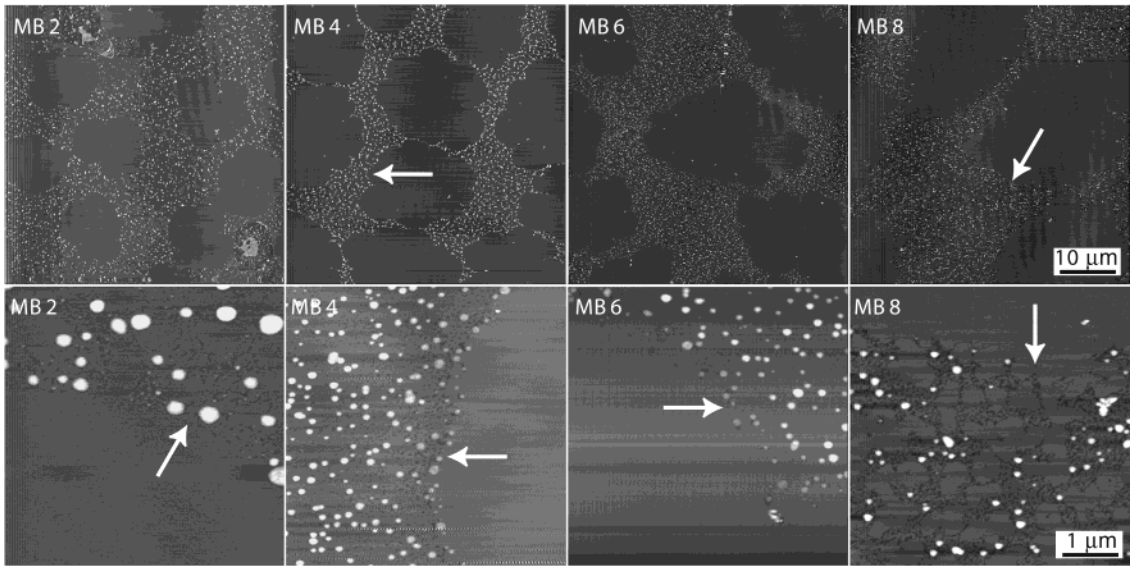

Figure 8. AFM images of deposited monolayers on mica surfaces of different lipid/dSP-B_{1-25} mixtures. The monolayers were deposited at 40 mN/m from pure water at 25.0 °C (above the plateaus in the isotherms shown in Figure 1). The top row shows 50 μm × 50 μm images which show coexistence of condensed and fluid phases, while the bottom row shows higher resolution 5 μm × 5 μm images. The characteristic flower shape of the condensed-phase domains is still visible at the arrows, but the contrast is due to the high density of nanosilos in the continuous phase. The higher magnification images show that there is no longer a height difference between the condensed-phase domains and the continuous phase. The nanosilos are from 50 to 300 nm in diameter and from 5 to 8 nm in height. The arrows show the borders between the continuous phase and condensed-phase domains.

from the absence of the fluid POPG (the lower resolution micrograph is not shown here). A significantly lower density of nanosilos is observed as compared to Figure 8, and the height of the fluid phase is now lower than that of the condensed phase.

For a DPPC/POPG/dSP-B_{1-25} (75/15/10) monolayer (Figure 9B), nanosilos were plentiful but the area fraction of the condensed phase was greatly reduced. The condensed domains were difficult to detect with either BAM or fluorescence microscopy, but the AFM images show submicron condensed-phase domains. This observation is consistent with previous work showing that PA promotes the formation of condensed phases in DPPC monolayers, effectively lowering the transition temperature of the films.[37−39,50]

Figure 9C−E shows AFM images of monolayers of DPPC/dSP-B_{1-25}, PA/dSP-B_{1-25}, and POPG/dSP-B_{1-25}, respectively. For the mixtures of DPPC/dSP-B_{1-25} (Figure 9C) and PA/dSP-B_{1-25} (Figure 9D), the condensed phase is dominant and there is little fluid phase. Nanosilos were rare, and the fluid phase is of lower height than the condensed phase. The fluid phase also shows a granular texture, which may be the concentration of the dSP-B_{1-25} in this phase.[32] For POPG/dSP-B_{1-25} (Figure 9E), however, nanosilos are plentiful and uniformly distributed across the film. Higher magnification images indicated that the nanosilos were again between 50 and 300 nm in diameter and from 5 to 8 nm in height. This confirms the central importance of POPG in nanosilo formation.

Figure 10 shows AFM images of DPPC/POPG/PA (75/15/8) mixtures with weight fractions of dSP-B_{1-25} ranging from 0 to 10 wt %. Nanosilos occur in all monolayers that contained dSP-B_{1-25}. The lateral dimensions of the nanosilos increased with increasing dSP-B_{1-25}, although the number of nanosilos remained roughly constant. To verify that the silos were not an artifact from the mica substrate, we also deposited monolayers on silicon wafers (Figure 11B). On silicon substrates, the nanosilos' height and density are similar to those on mica substrates (Figure 11A); hence, the substrate plays no role in the size and number of nanosilos.

Discussion

Proper pulmonary function requires low surface tensions at the end of expiration to minimize the work of

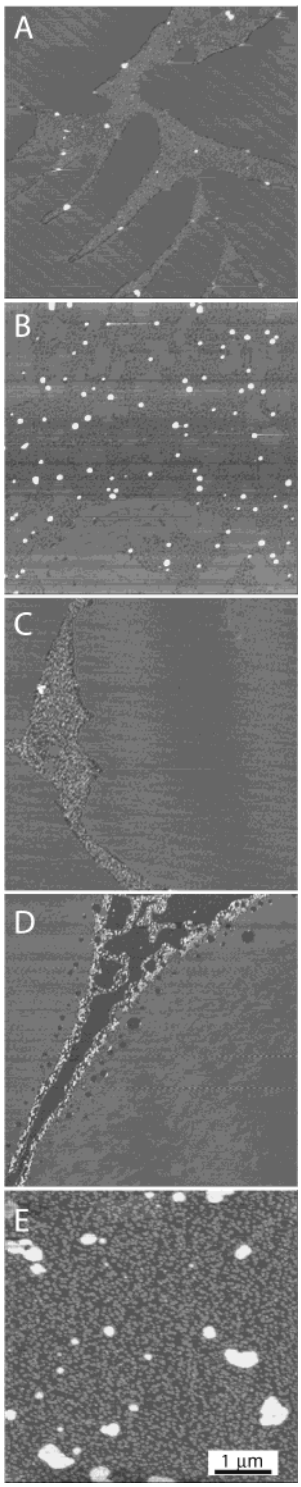

Figure 9. AFM images of deposited monolayers on mica of various lipid mixtures with dSP-B_{1-25}. The monolayers were also deposited on pure water at 40 mN/m and 25.0 °C as in Figure 8. (A) DPPC/PA/dSP-B_{1-25} (75/8/10, w/w/w). (B) DPPC/POPG/dSP-B_{1-25} (75/15/10). Nanosilos are present in the continuous phase as in Figure 8. (C) DPPC/dSP-B_{1-25}. (D) PA/dSP-B_{1-25}. (E) POPG/dSP-B_{1-25}. Only the systems with POPG and dSP-B_{1-25} show the formation of nanosilos (images B and E).

breathing.[51,52] This would seem to require that lung surfactant form rigid monolayers capable of low surface tension on compression. However, lung surfactant monolayers also must be fluid enough to spread rapidly during the expansion of the interface that accompanies inspiration. While the individual components of lung surfactant are good at either lowering surface tension (DPPC, especially when mixed with PA) or fluidizing the monolayer (unsaturated PG, proteins), *no* single lipid or protein exhibits both properties.

The multiplicity of requirements of lung surfactant monolayers has led to the squeeze-out theory of lung surfactant function: the unsaturated lipids and proteins in lung surfactant are selectively removed or squeezed-out from the monolayer during compression, leading to a DPPC-enriched monolayer capable of low surface tension.[1] Simple lipid mixtures do exhibit an irreversible squeeze-out of fluid lipids (generally unsaturated lipids above the critical temperature) from monolayers that also contain condensed-phase lipids (generally saturated lipids below the critical temperature).[31] However, in vitro studies of captive[41,53,54] and pulsating[55] air bubbles in contact with aqueous surfactant show that the necessary mass transfer to the interface requires that the surfactant remain within a few nanometers of the interface. Hence, current thought is that the lipids and proteins squeezed-out from the monolayer occupy a "surface-associated reservoir" near the interface.[41] In vivo, electron microscopy has shown areas within alveoli that have discontinuous multilayer or globular patches along with continuous monolayers.[41,56,57]

From AFM images, it appears that part of this surface-associated reservoir consists of 50−300 nm diameter patches about 5−10 nm thick in both bovine extract surfactant and in our model synthetic surfactant with a SP-B peptide. From the model surfactant, it is clear that the formation of the nanosilos requires the presence of both POPG and dSP-B_{1-25}. Previous studies have shown indirectly that there are specific interactions between PG and SP-B, the only protein of lung surfactant absolutely required for postnatal survival.[21,28,31,32,34] The fact that plateaus in the isotherms occur only for SP-B-containing monolayers indicates that these plateaus are due to SP-B. The extent of the plateaus depends on the POPG concentration in the monolayers (and likely on SP-C[21]), which argues that the plateaus arise from interactions between POPG and SP-B leading to the formation of the nanosilos. These nanosilos are reversibly reincorporated into the monolayer on expansion to lower surface pressures, which should help maintain the overall monolayer composition at low surface pressures. The same features are observed after expansion and recompression cycles. If POPG is simply squeezed-out from the monolayer without being held in a nanosilo, it likely does not reincorporate on expansion.[31]

It has been already predicted[58−60] that the surfactant proteins have to be at least partially removed from the monolayer along with a fraction of the lipids, based on film balance measurements and calculations of the mean

(51) Schürch, S.; Goerke, J.; Clements, J. A. *Proc. Natl. Acad. Sci. U.S.A.* **1976**, *73*, 4698−4702.
(52) Schürch, S.; Goerke, J.; Clements, J. A. *Proc. Natl. Acad. Sci. U.S.A.* **1978**, *75*, 3417−3421.
(53) Ingenito, E. P.; Mark, L.; Morris, J.; Espinosa, F. F.; Kamm, R. D.; Johnson, M. *J. Appl. Physiol.* **1999**, *86*, 1702−1714.
(54) Ingenito, E. P.; Mora, R.; Mark, L. *Am. J. Respir. Crit. Care Med.* **2000**, *161*, 831−838.
(55) Krueger, M. A.; Gaver, D. P., III. *J. Colloid Interface Sci.* **2000**, *229*, 353−364.
(56) Bastacky, J.; Lee, C. Y.; Goerke, J.; Koushafar, H.; Yager, D.; Speed, T. P.; Chen, Y.; Clements, J. A. *J. Appl. Physiol.* **1995**, *79*, 1615−1628.
(57) Tchoreloff, P.; Denizot, B.; Proust, J.; Gulik, A.; Puisieux, F. *Congr. Int. Technol. Pharm., 5th* **1989**, *3*, 41−50.
(58) Taneva, S.; Keough, K. M. W. *Biophys. J.* **1994**, *66*, 1137−1148.
(59) Taneva, S.; Keough, K. M. W. *Biophys. J.* **1994**, *66*, 1149−1157.
(60) Taneva, S.; Keough, K. M. W. *Biophys. J.* **1994**, *66*, 1158−1166.

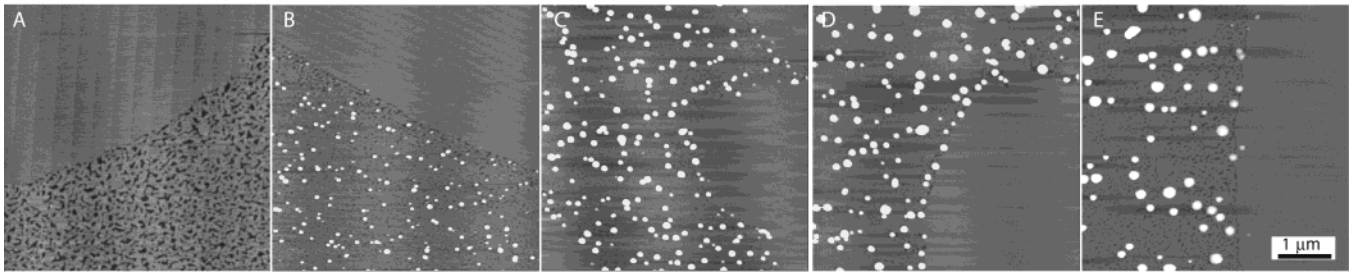

Figure 10. AFM images of DPPC/POPG/PA (75/15/8 w/w/w) monolayers deposited on mica surfaces with different amounts of dSP-B_{1-25}. The monolayers were deposited on pure water at 40 mN/m and 25.0 °C. (A) 0% dSP-B_{1-25}. (B) 2.5% dSP-B_{1-25}. This weight concentration corresponds most closely to that in Survanta, and the size and density of the nanosilos is most similar to those in Figure 3. (C) 5% dSP-B_{1-25}. (D) 7.5% dSP-B_{1-25}. (E) 10% dSP-B_{1-25}. The micrographs show that the lateral dimensions of the nanosilos increase as the amount of dSP-B_{1-25} increases, which indicates a correlation between nanosilo size and SP-B_{1-25} concentration.

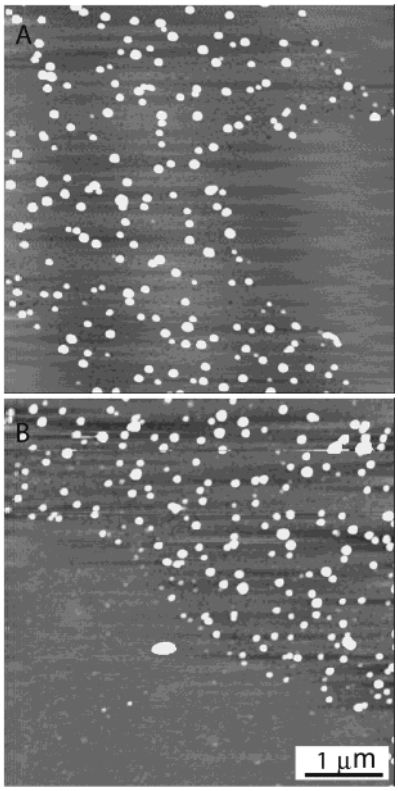

Figure 11. AFM images of monolayers (DPPC/POPG/PA/dSP-B_{1-25} (75/15/8/10)) deposited at 40 mN/m on pure water at 25.0 °C on freshly cleaved mica and oxidized silicon wafers. Both substrates give the same size and density of nanosilos.

area per molecule. Using external reflection−absorption infrared spectroscopy, Pastrana-Rios et al. found a loss of SP-B from the monolayer above a surface pressure of 40 mN/m, which was irreversible for a pure DPPC film but reversible if POPG was present.[61]

The nanosilo structure shows how the interactions between POPG and SP-B can retain both protein and fluid lipid in the immediate vicinity of the monolayer at high surface pressure, which allows both molecules to reincorporate in the monolayer at lower pressure. The nanosilos form reversibly during the plateau in the pressure−area isotherm, which is at a lower surface pressure than the collapse pressure of POPG.[31] This transition moves some fraction of the POPG and SP-B from the 2-D monolayer to form a 3-D POPG−SP-B reservoir. The formation of nanosilos does not require a high fraction of SP-B; nanosilos were found in synthetic mixtures containing only 2.5 wt % dSP-B_{1-25} and POPG, as well as in the commercial replacement surfactant Survanta, which contains less than 1 wt % native SP-B.[7] However, the density of nanosilos is proportional to the concentration of SP-B and depends on the fraction of POPG in the monolayer.

The observation that both SP-B and POPG are required for nanosilo formation might explain why SP-B is crucial to lung surfactant performance[12,13] and why a lack of PG correlates with respiratory distress syndrome.[26] Without SP-B and/or POPG, nanosilos do not form; therefore, the lung surfactant monolayers are not stable at higher pressure and the monolayer composition would likely change during successive compression−expansion cycles, which implies negative changes in surfactant performance.

Conclusions

PG has been proved to be a very useful biochemical marker for the maturity of the lung surfactant system in the developing fetus,[1,27] and SP-B has been shown to concentrate and interact specifically with PG.[28,34] In this study, we used DPPC/POPG and PA with or without dSP-B_{1-25}, a homodimeric peptide mimic, as a model lung surfactant. A systematic examination of the mixed monolayers containing various fractions of DPPC, POPG, PA, and dSP-B_{1-25} showed that only monolayers containing dSP-B_{1-25} showed plateaus in the pressure−area isotherm similar to those of Survanta, a bovine extract replacement surfactant that contains the native surfactant proteins.

BAM and AFM images showed that at surface pressures at and above the plateau pressure (>30−40 mN/m), monolayers containing POPG and SP-B_{1-25} form a 3-D structure we have called nanosilos. The nanosilos are from 50 to 300 nm in diameter and from 5 to 8 nm in height. These nanosilos are not observed in monolayers transferred at surface pressures below the plateau. Very similar structures are observed in Survanta monolayers deposited at surface pressures above its plateau pressure, suggesting that (1) these isotherm and morphological features in Survanta are due to the presence of unsaturated phosphatidylglycerol and SP-B and (2) at least these features of native SP-B can be mimicked by the dSP-B_{1-25} peptide. The net effect of the nanosilo is to stabilize the monolayer composition by trapping POPG and SP-B in three-dimensional surface-associated aggregates at high surface pressures so that they can be easily reincorporated into the monolayer at lower surface pressures.

(61) Pastrana-Rios, B.; Flach, C. R.; Brauner, J. W.; Mautone, A. J.; Mendelsohn, R. *Biochemistry* **1994**, *33*, 5121−5127.
(62) Richards, F. M. *Annu. Rev. Biophys. Bioeng.* **1977**, *6*, 151−176.

Acknowledgment. The authors acknowledge financial support from National Institutes of Health Grant HL-51177 and the University of California Tobacco Related Disease Research Program, Grant Nos. 8RT-0077, 8DT-0171, and 11RT-0222. H.E.W. was supported by a National Institutes of Health postdoctoral fellowship. J.D. is grateful for technical support from Mr. R. Stuber, D. Rehn, and M. Wrocklage of the Physics Machine Shop at UCSB.

Abbreviations

DPPC	dipalmitoylphosphatidylcholine
POPG	palmitoyloleoylphosphatidylglycerol
PG	phosphatidylglycerol
PA	palmitic acid
dSP-B_{1-25}	a peptide based on the N-terminus of SP-B of the first 25 amino acid sequence in dimer format

Mixture Labels (All Components in Weight Ratio)

MA1	DPPC/POPG/PA = 45/45/8
MA2	DPPC/POPG/PA = 50/40/8
MA3	DPPC/POPG/PA = 55/35/8
MA4	DPPC/POPG/PA = 60/30/8
MA5	DPPC/POPG/PA = 65/25/8
MA6	DPPC/POPG/PA = 70/20/8
MA7	DPPC/POPG/PA = 75/15/8
MA8	DPPC/POPG/PA = 80/10/8
MB1	DPPC/POPG/PA/dSP-B_{1-25} = 45/45/8/10
MB2	DPPC/POPG/PA/dSP-B_{1-25} = 50/40/8/10
MB3	DPPC/POPG/PA/dSP-B_{1-25} = 55/35/8/10
MB4	DPPC/POPG/PA/dSP-B_{1-25} = 60/30/8/10
MB5	DPPC/POPG/PA/dSP-B_{1-25} = 65/25/8/10
MB6	DPPC/POPG/PA/dSP-B_{1-25} = 70/20/8/10
MB7	DPPC/POPG/PA/dSP-B_{1-25} = 75/15/8/10
MB8	DPPC/POPG/PA/dSP-B_{1-25} = 80/10/8/10

LA0261794